VNU Journal of Science: Mathematics - Physics
Journal homepage: https://js.vnu.edu.vn/MaP

Original Article

Study on Microwave Absorption Performance of Submicron $SrFe_{12}O_{19}$ Particles Prepared by Hydrothermal Method

Tran Thi Viet Nga[1,*], Nguyen Van Quang[2], To Thanh Loan[1], Hoang Manh Chung[3], Luong Ngoc Anh[1]

[1]*School of Materials Science and Engineering, Hanoi University of Science and Technology, 1 Dai Co Viet, Hanoi, Vietnam*

[2]*School of Engineering Physic, Hanoi University of Science and Technology, 1 Dai Co Viet, Hanoi, Vietnam*

[3]*Thai Nguyen University of Technology, 666, 3-2 Road, Thai Nguyen, Vietnam*

Received 23 May 2023
Revised 14 July 2023; Accepted 18 March 2024

Abstract: Strontium hexaferrite ($SrFe_{12}O_{19}$) materials were synthesized through the hydrothermal method with conditions at R= (Fe^{3+}+ Sr^{2+})/(OH^-) ratio of 2 to 4 (R ratio of 1/2, 1/3 and 1/4 were, respectively abbreviated to M2, M3 and M4). R has been examined by employing $Fe(NO_3)_3$ and $Sr(NO_3)_2$ as the initial materials. The effects of R ratio on the structure, particle size, magnetic and microwave-absorbing properties of the samples were studied. The coercivity and saturation magnetization of M4 sample reach 5.2 kOe and 58.7 emu/g, respectively. The optimal reflection loss of the M4 at the thickness of 1.5 mm reached a value as large as - 48.27 dB in the frequency range of 2 to 18 GHz. The improvement in microwave absorption performance of M4 sample compared to M2 and M3 was mainly resulted from the increased magnetic properties with increasing R ratio.

Keywords: Hydrothermal method; microwave absorption properties, hexaferrite.

1. Introduction

The development of science and technology brings many benefits to human life. The rapid development of electromagnetic technology and electronic devices brings many conveniences to people's lives. However, the application of electromagnetic waves by electronic devices also causes

* Corresponding author.
E-mail address: vietnga@itims.edu.vn

https//doi.org/10.25073/2588-1124/vnumap.4851

hazards to the environment and human health. Electromagnetic pollution proposes a certain threat to the survival of the human body and other animals and plants, and electromagnetic interference will make precision electronic equipment go wrong, causing negative impacts on medical, manufacturing, communication, and other industries [1-2]. Moreover, in the military field, to ensure safety and security, making equipment and weapons invisible to radar systems is always a focus [3]. Therefore, in recent years, the studies on the microwave absorption materials (MAMs) have become a hot research topic. The recent studies mainly focused on development material with advantages such as light weight, thin thickness, high efficiency absorption and broadened absorption band [4-7]. For microwave absorption materials, morphology plays an important role. The previous studies have shown that the flake-like absorbents can produce a stronger interfacial polarization and show enhanced microwave absorption properties because of larger surface areas [8]. Hexaferrites are hard ferrites, consisting of high coercivity, high complex permeability and good chemical stability, which make them suitable for the representative of magnetic loss type absorbers [9]. In addition, the crystalline hexaferrite is liable to be flake-like. So many studies of hexaferrite have been reported on determination of its microwave absorbing properties in X-band and K_u band frequencies.

In this work, $SrFe_{12}O_{19}$ samples were synthesized by hydrothermal method. We systematically studied the influence of an alkaline environment (NaOH) with the molar ratio (R) of 2 , 3 and 4 on the structure, magnetic properties of $SrFe_{12}O_{19}$ particles prepared by hydrothermal method. The relation between morphology, magnetic properties and microwave absorption properties of materials have been investigated.

2. Experimental Procedure

The chemical precursors used for these experiments are of $Fe(NO_3)_3$. $9H_2O$, $Sr(NO_3)_2$ and NaOH. The first, a salt mixture containing $Fe(NO_3)_3$ and $Sr(NO_3)_2$ was dissolved in deionized water with molar ratio of Fe^{3+}: Sr^{2+} = 12/1. Then, NaOH solution was slowly dropped into the solution. The solutions were stirred at 1,000 rpm for 30 min to form a precipitate. Then, this mixture was transferred in a Teflon-lined stainless-steel autoclave with a 100 ml capacity at 180 ^oC and stored for 6 h in an oven. Finally, the precipitated products were washed with deionized water and then dried at 60 ^oC for 6 h.

The as-synthesised particles were calcined at 800 ^oC for 5 h. The sample whose was added NaOH solution with the R= (Fe^{3+}+ Sr^{2+})/(OH^-) molar ratio of 1/2, 1/3 and 1/4 were labelled as M2, M3 and M4. Figure 1 shows the synthesis and characterization of the $SrFe_{12}O_{19}$ particles.

Figure 1. Flowchart for preparation of $SrFe_{12}O_{19}$ particles.

The crystalline structures of the obtained particles were identified via X-ray powder diffraction (XRD) using D2 Phaser Bruker diffractometer. The morphology and the particle size were observed via a scanning electron microscopy (SEM, JEOL-JSM 7600F). The Raman spectra were obtained using Raman spectrometer in the 200-1,000 cm^{-1} range. The magnetic properties were measured using a vibrating sample magnetometer (VSM, Lake-shore 7410) with applied magnetic fields of up to 15 kOe. The samples were mixed with paraffin and pressed into a toroid with an outer diameter of 7 mm and an inner diameter of 3.04 mm. Microwave absorption samples were pressed with different lengths and determined by the vector network analyser (Vector Keysight N5242) using a coaxial method in the frequency range of 2-18 GHz. Finally, the microwave absorption characteristic was evaluated using transmission line theory.

3. Results and Discussion

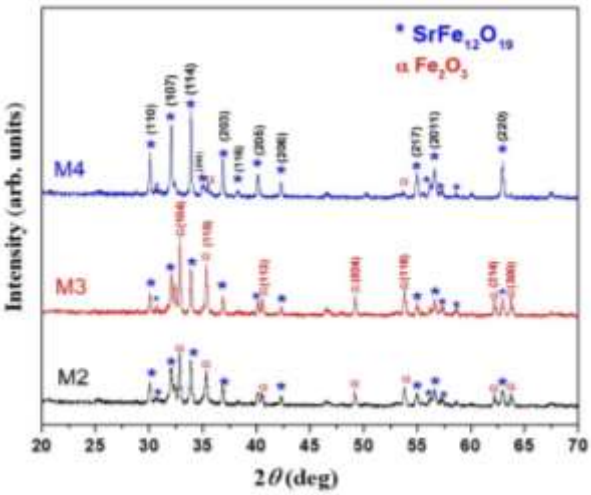

Figure. 2. X-ray powder diffraction patterns of the samples synthesized hydrothermally with different ratios of $(Fe^{3+}+ Sr^{2+})/(OH^{-})$.

The $(Fe^{3+}+ Sr^{2+})/(OH^{-})$ ratio (R) was initially varied as 1/2, 1/3 and 1/4 to investigate its effect on the structure, particle size and morphology. X- ray diffraction patterns of the as-synthesised powders are shown in Figure 2. It can be clearly seen that the M2 and M3 samples contained both the $SrFe_{12}O_{19}$ phase and α-Fe_2O_3 phase characterizing by diffraction peaks of the planes with Miller indices of (104), (110), (113), (024), (116), (214) and (300). With R = 1/4, in the sample there is only a small percentage (< 0.5%) of α-Fe_2O_3, which could be ignored.

Thus, the sample with R = 1/4 was confirmed to have a single crystalline phase. Therefore, for the M2 and M3 samples, under the current hydrothermal conditions and after calcination, the reaction between Fe^{3+} and Sr^{2+} does not occur completely, leading to the presence of the α-Fe_2O_3 phase in these samples. This observation was also reported by other author [10-12] and may be attributed to the occurrence of local combustion during the annealing of this reaction:

$$Fe(OH)_3 = Fe_2O_3 + H_2O \quad (1)$$

With decreasing $(Fe^{3+}+ Sr^{2+})/(OH^{-})$ ratio, the amount of $SrFe_{12}O_{19}$ phase increases and then becomes the predominant phase. The main phase formation process occurs according to the following equation:

$$FeOOH + Sr(OH)_2 \rightarrow SrO.6Fe_2O_3 + 7H_2O \quad (2)$$

The lattice parameters (*a*, *c*), unit cell volume (*V*) and crystallite sizes (*D*) are listed in Table 1. These lattice parameters of $SrFe_{12}O_{19}$ tend to increase with decreasing in $(Fe^{3+}+ Sr^{2+})/(OH^-)$ ratio. This resulted in complete reaction between Fe^{3+} and Sr^{2+} when decreasing in $(Fe^{3+}+ Sr^{2+})/(OH^-)$ ratio, indicated by decreasing of α-Fe_2O_3 phase. This result is in agreement with those reported by Wang [11, 12].

Table 1. The lattice parameters (*a*, *c*), unit cell volume (*V*) and crystallite sizes (*D*)

Sample	$SrFe_{12}O_{19}$				α- Fe_2O_3			
	a (Å)	*c* (Å)	*V* (Å^3)	*D* (nm)	*a* (Å)	*c* (Å)	*V* (Å^3)	*D* (nm)
M2	5.7821	23.034	666.916	45.31	5.033	13.739	301.397	37.403
M3	5.7837	23.087	668.821	46.19	5.037	13.702	301.604	37.384
M4	5.7901	23.154	672.247	46.62	-	-	-	-

Figure 3 shows the SEM images of the samples. From this figureOne can see that plate-like particles were obtained for all the samples. For the samples with *R* = 1/2 and 1/3, the average particles size was evenly distributed in the range of 20 nm to 120 nm. From the morphologies of the samples, one cannot distinguish the differences between α-Fe_2O_3 and $SrFe_{12}O_{19}$ particles. Meanwhile, the sample with *R* = 1/4, it could be seen that sample consisted of numerous highly uniform plate-like particles and the average diameter range from 80-100 nm.

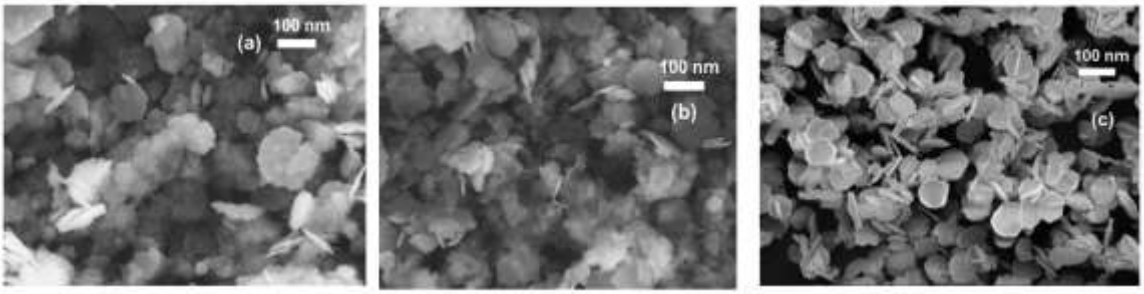

Figure 3. SEM images of (a) M2, (b) M3 and (c) M4.

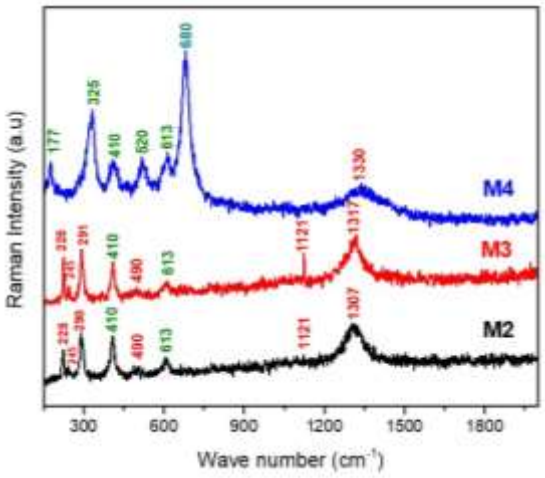

Figure 4. Raman spectrum of samples.

The Raman spectra of samples were measured at room temperature to confirm the presence of the crystalline phases in M2, M3 and M4 samples. The results are shown in Fig. 4, six modes of α-Fe_2O_3 at the wavenumbers of 225 cm^{-1}, 245 cm^{-1}, 290 cm^{-1}, 490 cm^{-1}, 1121 cm^{-1} and 1307 cm^{-1} occurredfor M2 and M3 samples. Whereas, for M4 sample there is only one mode of α-Fe_2O_3 at a wavelength of 1330 cm^{-1}. Modes of $SrFe_{12}O_{19}$ are found in all samples. All modes have shifting tendency toward a high wave number.

In Figure 5 the hysteresis loops of the samples are compared. For M2 and M3 samples, although their crystallo-graphically compose of $SrFe_{12}O_{19}$ phase and α-Fe_2O_3 phase (Fig. 2), the hysteresis loop shows a single-phase magnetization, implying that the $SrFe_{12}O_{19}$ phase and α-Fe_2O_3 phase are exchange coupled. The hysteresis loops of samples will exhibit a typical "bee-waist" if the soft phase magnetization is not tightly coupled to the hard phase. In the case of effective exchange coupling, there exists only one peak, indicating that one step of magnetic reversal was completed in the nanocomposite samples. The magnetic exchange coupling of the samples could be further investigated by the dM/dH of the demagnetization curves (Figure 6). If the magnetic phases are uncoupled or have weak coupling, two different peaks will be observed in low and high field. A low peak in intensity which appear at the low field of the switching field distribution curves shows a relatively high degree of exchange coupling [13]. In this work, the dM/dH curves of samples with different R ratios exhibit two peaks. However, the peak intensity in low field becomes weak with the decrease in R ratio, indicating the improvement of the exchange coupling effect by occurring of main phase formation $SrFe_{12}O_{19}$. Thus, for M2 and M3 samples, though crystallographically they exhibit two phase behaviour, magnetically it gives a good single step loop. The coercivity H_C and saturation magnetization M_S increases with increasing (Fe^{3+}+ Sr^{2+})/(OH^-) ratio. This may be attributed mainly to the improvement of the hexaferrite crystalline. The coercivity and saturation magnetization of M4 sample reach 5.2 kOe and 58.7 emu/g, respectively.

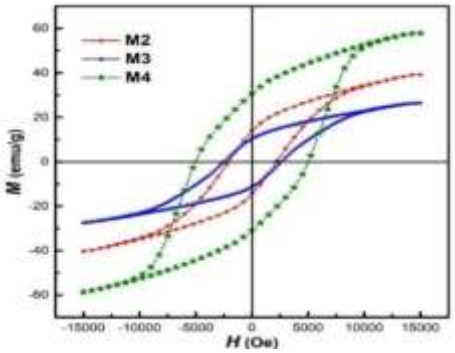

Figure 5. Hysteresis loops of M2, M3 and M4 samples.

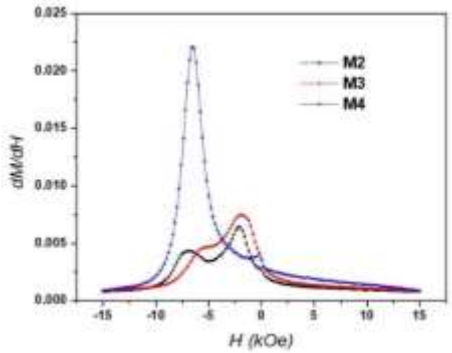

Figure 6. The dM/dH curves of samples with different R ratios.

The reflection loss pattern of samples as a function of frequency is shown in Figure 7. It is clearly seen that all samples show excellent microwave absorption properties. For M2 sample, the minimum reflection loss (*RL)* reached -43.56 dB at 15.61 GHz with a thickness of 3.5 mm. With a thickness 1.5 mm, the M2 pellet shows very low value of *RL*, -10.87 dB. However, by increasing the thickness in this sample, the *RL* is observed to increase. The bandwidth corresponding to *RL* below -10 dB for M2 increase with thickness. At the same thickness, the bandwidth of M3 is higher than that of M2. The minimum *RL* of M3 reach -42.07 dB at 16.24 GHz with a thickness of 3.0 mm.

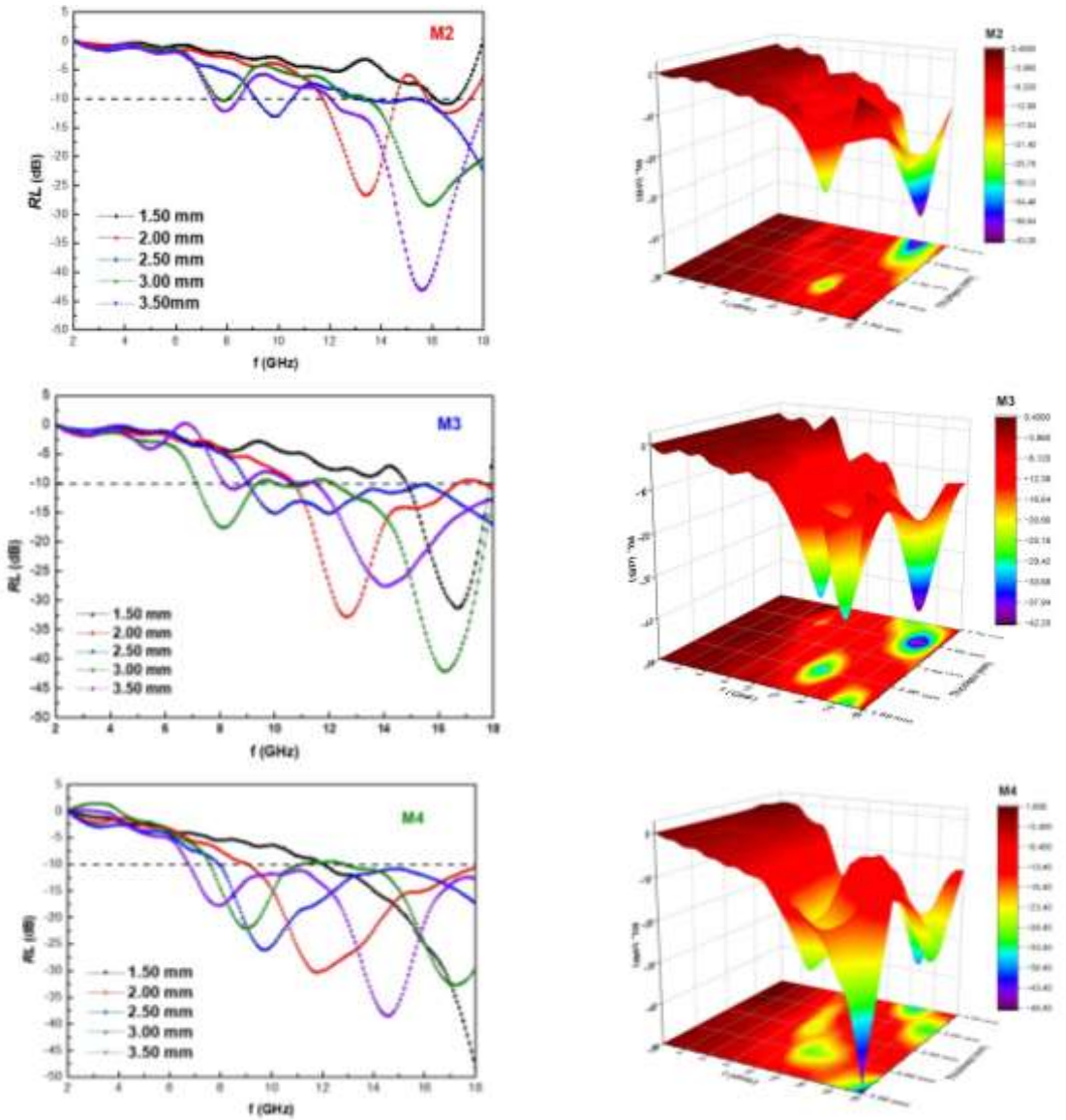

Figure 7. *RL* curves and corresponding 3D plots for M2, M3 and M4 samples.

The optimal results are observed for M4 sample having minimum *RL* of -48.27 dB at 18 GHz with a thickness of 1.5 mm. The bandwidth corresponding to *RL* below -10 dB for M4 with thicknesses of 1.5, 2.0, 2.5, 3.0 and 3.5 mm are 5.94, 9, 10.15, 8.8 and 11.33 GHz, respectively. The achievement is

due to the improvement of crystal structure of the M4 sample when increasing of $(Fe^{3+}+ Sr^{2+})/(OH^-)$ ratio. In reality, microwave absorption materials consist of two main types: dielectric loss and magnetic loss. Hexaferrite with excellent natural resonance loss and magnetic hysteresis loss shows high complex permeability values and is a representative material for magnetic loss type absorbers. All samples have a flake shape, however, the presence of the α- Fe_2O_3 phase in M2 and M3 samples reduces the magnetic properties of these samples compared to the M4 sample. Therefore, the microwave absorption properties of the M2 and M3 samples are lower than those of the M4 sample. Garg et al., [14] prepared strontium hexaferrite particles using auto combustion method where the minimum reflection loss reaches -14.44 dB at 9.37 GHz for effective thickness of 2.6 mm. Similarly, the RGO/$BaFe_{12}O_{19}$/Fe_3O_4 composites were developed by Jiao et al., [4] shows optimized results at thickness of 1.8 mm having -10 dB bandwidth of 5.68 GHz and reflection loss reach -46.04 dB at 15.6 GHz. These results are 45% and 5% lower than the M4 sample for the same thickness, respectively. The improvement in microwave absorption properties of our samples compared to these studies is due to the flake's morphology of synthesized particles (Figure 3). Among these absorbents, flakes with larger surface areas can produce a stronger interfacial polarization and show enhanced microwave absorption. The minimum reflection loss *RL* and the absorption bandwidth of samples are listed in Table 2.

Table 2. The minimum reflection loss *RL* and the absorption bandwidth of M2, M3 and M4 samples

Sample	*RL* (dB)	*f* (GHz)	Absorption bandwidth (GHz)	Thickness (mm)
M2	-10.87	16.56	0.95	1.50
	-26.96	13.44	4.57	2.00
	-21.98	18	4.03	2.50
	-28.45	15.92	8.2	3.00
	-43.56	15.61	6	3.50
M3	-31.29	16.72	2.94	1.50
	-32.77	12.64	6	2.00
	-16.98	18	8.98	2.50
	-42.07	16.24	6.57	3.00
	-27.52	14	6.47	3.50
M4	-48.27	18	5.94	1.50
	-30.56	11.74	9	2.00
	-26.21	9.73	10.15	2.50
	-32.72	17.19	8.8	3.00
	-38.83	14.57	11.33	3.50

Conclusion

In summary, we reported the fabrication of $SrFe_{12}O_{19}$ particles with a plate-like structure using the hydrothermal method. The coercivity H_C and saturation magnetization M_S increases with increasing $(Fe^{3+}+ Sr^{2+})/(OH^-)$ molar ratio. This may be attributed mainly due to the improvement of the hexaferrite crystalline. The optimal reflection loss of the M4 at the thickness of 1.5 mm reaches -48.27 dB in the frequency range of 2 to18 GHz. The improvement in microwave absorption performance of M4 sample compared to M2 and M3 is mainly resulted from the increased magnetic properties with increasing the molar ratio. In addition, the flakes morphology of synthesized particles also significantly affects their microwave absorption properties.

Acknowledgment

This research was financially supported by the Ministry of Education and Training under Project No. B2022-BKA-17.

References

[1] X. Lin et al., Connecting of Conjugate Microporous Polymer Nanoparticles by Polypyrrole Via Sulfonic Acid Doping to Form Conductive Nanocomposites for Excellent Microwaves Absorption,Composites Science and Technology, Vol. 221, No. 2, 2022, pp. 109350, https//doi.org/10.1016/j.compscitech.2022.109350.

[2] P. Liu, C. Zhu, S. Gao, C. Guan, Y. Huang, W. He, N-doped Porous Carbon Nanoplates Embedded with CoS_2 Vertically Anchored on Carbon Cloths for Flexible and Ultrahigh Microwave Absorption, Carbon, Vol. 163, 2020, pp. 348-359, https//doi.org/10.1016/j.carbon.2020.03.041.

[3] M. Green, X. Chen, Recent Progress of Nanomaterials for Microwave Absorption, Journal of Materiomics, Vol. 5, No. 4, 2019, pp. 503-541, https//doi.org/0.1016/j.jmat.2019.07.003.

[4] S. Jiao et al., RGO/BaFe12O19/Fe3O4 Nanocomposite as Microwave Absorbent with Lamellar Structures and Improved Polarization Interfaces, Materials Research Bulletin, Vol. 108, 2018, pp. 89-95, https//doi.org/10.1016/j.materresbull.2018.08.014.

[5] Z. Zhang, X. Liu, X. Wang, Y. Wu, Y. Liu, Electromagnetic and Microwave Absorption Properties of FeSr 0.8La 0.2Fe 11.8Co 0.2O 19 Shell-core Composites, Journal of Magnetism and Magnetic Materials, Vol. 324, No. 13, 2012, pp. 2177-2182, https//doi.org/10.1016/j.jmmm.2012.02.107.

[6] H. Yang, T. Ye, Y. Lin, M. Liu, Preparation and Microwave Absorption Property of Graphene/BaFe 12 O 19 /CoFe 2 O 4 Nanocomposite, Applied Surface Science, Vol. 357, 2015, pp. 1289-1293, https//doi.org/10.1016/j.apsusc.2015.09.147.

[7] G. Mu, N. Chen, X. Pan, H. Shen, M. Gu, Preparation and Microwave Absorption Properties of Barium Ferrite Nanorods, Materials Letters, Vol. 62, No. 6-7, 2008, pp. 840-842, https//doi.org/10.1016/j.matlet.2007.06.074.

[8] H. Lv, Y. Guo, G. Wu, G. Ji, Y. Zhao, Z. J. Xu, Interface Polarization Strategy to Solve Electromagnetic Wave Interference Issue, Vol. 9, No. 6. 2017.

[9] P. Saravanan et al., Effect of Fe Layer Thickness and Fe/Co Intermixing on the Magnetic Properties of Sm-Co/Fe Bilayer Exchange-Spring Magnets, Journal of Physics D: Applied Physics, Vol. 46, No. 15, 2013, https//doi.org/10.1088/0022-3727/46/15/155002.

[10] X. Liu, J. Wang, L. M. Gan, S. C. Ng, Improving the Magnetic Properties of Hydrothermally Synthesized Barium Ferrite, Journal of Magnetism and Magnetic Materials, vol. 195, No. 2, 1999, pp. 452-459, https//doi.org/10.1016/S0304-8853(99)00123-7.

[11] J. Wang, C. Ponton, R. Grössinger, I. Harris, A Study of La-substituted Strontium Hexaferrite by Hydrothermal Synthesis, Journal of Alloys and Compounds, Vol. 369, No. 1-2, 2003, pp. 170-177, https//doi.org/10.1016/j.jallcom.2003.09.097.

[12] J. F. Wang, C. B. Ponton, I. R. Harris, A Study of Pr-Substituted Strontium Hexaferrite by Hydrothermal Synthesis, Journal of Alloys and Compounds, Vol. 403, No. 1-2, 2005, pp. 104-109, https//doi.org/10.1016/j.jallcom.2005.05.025.

[13] J. Liang, X. Wu, W. Wu, L. Chen, Y. Huang, Y. Huang, Improved Magnetic Properties of Sr0.93Sm0.10Fe11.97O19/Fe_3O_4 Composite Powders by Substitution of Sm and Magnetic Exchange Coupling Effect, Journal of Materials Science: Materials in Electronics, Vol. 31, No. 22, 2020, pp. 20400-20410, https//doi.org/10.1007/s10854-020-04559-1.

[14] A. Garg, S. Goel, N. Kumari, P. Soni, H. B. Baskey, S. Tyagi, Yttrium-doped Strontium Hexaferrite Particles for Microwave Absorption Application in X-band, Journal of Materials Science: Materials in Electronics, Vol. 31, No. 16, 2020, pp. 13746-13755, https//doi.org/10.1007/s10854-020-03934-2.